Journal of Magnetic Resonance 193 (2008) 297–304

Contents lists available at ScienceDirect

Journal of Magnetic Resonance

journal homepage: www.elsevier.com/locate/jmr

Saturation recovery EPR and ELDOR at *W*-band for spin labels

Wojciech Froncisz [a,b], Theodore G. Camenisch [a], Joseph J. Ratke [a], James R. Anderson [a], Witold K. Subczynski [a], Robert A. Strangeway [a,c], Jason W. Sidabras [a], James S. Hyde [a,*]

[a] Department of Biophysics, Medical College of Wisconsin, 8701 Watertown Plank Road, P.O. Box 26509, Milwaukee, WI 53226-0509, USA
[b] Jagiellonian University, Krakow, Poland
[c] Milwaukee School of Engineering, Milwaukee, WI, USA

ARTICLE INFO

Article history:
Received 7 September 2007
Revised 30 April 2008
Available online 20 May 2008

Keywords:
EPR
W-band
Loop-gap resonator
Saturation recovery
ELDOR
Frequency translation
Spin label

ABSTRACT

A reference arm *W*-band (94 GHz) microwave bridge with two sample-irradiation arms for saturation recovery (SR) EPR and ELDOR experiments is described. Frequencies in each arm are derived from 2 GHz synthesizers that have a common time-base and are translated to 94 GHz in steps of 33 and 59 GHz. Intended applications are to nitroxide radical spin labels and spin probes in the liquid phase. An enabling technology is the use of a *W*-band loop-gap resonator (LGR) [J.W. Sidabras, R.R. Mett, W. Froncisz, T.G. Camenisch, J.R. Anderson, J.S. Hyde, Multipurpose EPR loop-gap resonator and cylindrical TE_{011} cavity for aqueous samples at 94 GHz, Rev. Sci. Instrum. 78 (2007) 034701]. The high efficiency parameter (8.2 $GW^{-1/2}$ with sample) permits the saturating pump pulse level to be just 5 mW or less. Applications of SR EPR and ELDOR to the hydrophilic spin labels 3-carbamoyl-2,2,5,5-tetra-methyl-3-pyrroline-1-yloxyl (CTPO) and 2,2,6,6,-tetramethyl-4-piperidone-1-oxyl (TEMPONE) are described in detail. In the SR ELDOR experiment, nitrogen nuclear relaxation as well as Heisenberg exchange transfer saturation from pumped to observed hyperfine transitions. SR ELDOR was found to be an essential method for measurements of saturation transfer rates for small molecules such as TEMPONE. Free induction decay (FID) signals for small nitroxides at *W*-band are also reported. Results are compared with multifrequency measurements of T_{1e} previously reported for these molecules in the range of 2–35 GHz [J.S. Hyde, J.-J. Yin, W.K. Subczynski, T.G. Camenisch, J.J. Ratke, W. Froncisz, Spin label EPR T_1 values using saturation recovery from 2 to 35 GHz. J. Phys. Chem. B 108 (2004) 9524–9529]. The values of T_{1e} decrease at 94 GHz relative to values at 35 GHz.

1. Introduction

1.1. Overview of saturation recovery EPR and ELDOR at *W*-band

A new pulse EPR instrument is described for use at 94 GHz (*W*-band). It is tailored for saturation recovery (SR) experiments where a saturating pulse changes the *z*-component of magnetization and the recovery to equilibrium is monitored by a weak observing microwave source. SR is the method of choice in EPR for measuring the electron spin–lattice relaxation time T_{1e}. The instrument can also be used for SR ELDOR. In this case, one of the EPR transitions in the spectrum is saturated and a second transition is observed. If a saturation transfer mechanism is active, the observed signal decreases at a saturation transfer rate and subsequently recovers with a time constant T_{1e}. Several reviews of ELDOR and SR EPR have been written [1–4].

Primarily, our interest in these experiments lies in the contribution that can be made to analysis of nitroxide radical spin-labeled systems in the aqueous phase. A principal application of SR is the measurement of oxygen transport, consumption, and accessibility to the spin-labeled site. Spin-label accessibility has been reviewed by Klug and Feix [5] and spin-label oximetry by Subczynski and Swartz [6].

The literature contains a number of papers on *W*-band EPR instrumentation. These are for the most part summarized in the treatise by Grinberg and Berliner [7]. Since publication of this book, the only article on high-field EPR instrumentation to the best of our knowledge is that of Ref. [8]. The papers by Wang et al. [9], Nilges et al. [10], and Hofer et al. [11] focus on continuous wave (CW) EPR, which is used for SR detection, and these papers have provided useful background in the development of the instrument described here. The others focus on spin-echo EPR, usually at cryogenic temperatures, and were less relevant.

Applications of high-field EPR to spin-labeled systems are reviewed by Earle and Smirnov [12].

The literature contains just three papers where SR ELDOR methods were applied to spin labels [13–15]. Partly, this is because of the increased complexity of the apparatus—there is an additional microwave frequency incident on the sample—and partly because

* Corresponding author. Fax: +1 414 456 6512.
E-mail address: jshyde@mcw.edu (J.S. Hyde).

1090-7807/$ - see front matter © 2008 Elsevier Inc. All rights reserved.
doi:10.1016/j.jmr.2008.05.008

of the relatively narrow bandwidth of resonators that must support two frequencies. The issue of bandwidth can be overcome using bimodal resonators with one mode tuned to a first frequency and the other to a second frequency, but resonators of this type are complex to build and use. In the new instrument, we use a *W*-band loop-gap resonator (LGR) that has a bandwidth of about 1 GHz [16]. One thesis of this paper is that *W*-band SR ELDOR is greatly facilitated by the high bandwidth of this resonator.

We have previously presented SR data acquired at *Q*-band [17]. The bridge that is described in that paper has multiple arms and also is suitable for SR ELDOR experiments, which have been performed at *Q*-band but as yet are unpublished. We have developed a *W*-band translation assembly that translates each of the multiple arms of the *Q*-band bridge to *W*-band, and have published one paper where this configuration was used [18]. It described microwave frequency-modulation experiments. As in the present paper, a *W*-band LGR was used. The SR experiment described here also benefits from the high bandwidth of this resonator.

This is the first report of SR EPR and SR ELDOR apparatus and experiments in the liquid phase at *W*-band.

1.2. Spin-label oximetry

Experiments on the hydrophilic spin probe 3-carbamoyl-2,2,5,5-tetramethyl-3-pyrroline-1-yloxyl (CTPO), compound I of Fig. 1, are described not only to illustrate features of the instrument but also because this is a widely used compound for spin-label oximetry. In an early paper, Backer et al. [19] used the resolution of the superhyperfine structure of compound II (4-carboxy-2.2.5.5-tetramethyl-3-imidazoline-3-oxide-1-oxyl) of Fig. 1 as an indicator of bimolecular collisions with dissolved O_2. Sarna et al. [20] seems to be the earliest report of the use of CTPO for oximetry, although Subczynski had previously developed a calibration curve (Ref. [20], Acknowledgment). They introduced a useful empirical parameter to characterize line broadening, the so-called *K* parameter. In a study of cellular respiration, Lai et al. [21] produced a careful calibration of this parameter. Hyde and Subczynski [22] realized that the superhyperfine pattern of CTPO arose not only from the methyl protons but also from the ring proton. There is an accidental degeneracy: this coupling is about 0.5 G, 2.5 times greater than the methyl proton coupling of 0.2 G. They suggested that simulation of the complete superhyperfine pattern was a better way to measure line broadening than use of the *K* parameter. Halpern et al. [23] introduced the use of ^{15}N CTPO with methyl deuterons and a ring proton. The resolution of the two-line feature from this proton served as a probe of bimolecular collisions with oxygen. *This molecule was used here*. Natural isotope abundance CTPO was also used. Results on 2,2,6,6-tetramethyl-4-piperidone-1-oxyl (TEMPONE) (compound III of Fig. 1), a nitroxide that has a six-member ring, are also reported as a control on results for CTPO, which has a five-member ring.

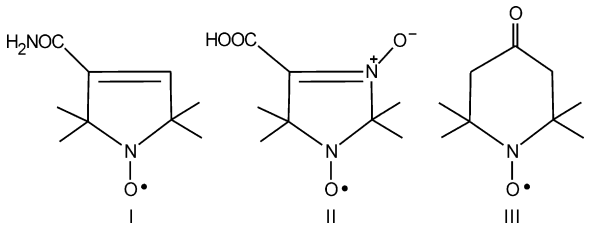

Fig. 1. Spin labels used in this study: (I) is known as CTPO and (III) as TEMPONE. Spin label (II) is discussed in the text.

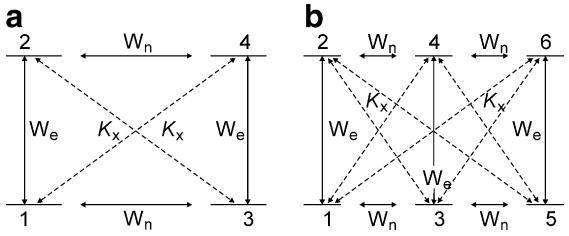

Fig. 2. Energy-level diagrams: (a) ^{15}N and (b) ^{14}N spin labels.

1.3. Summary of the theory of SR EPR and ELDOR of spin labels

Fig. 2 shows the energy-level diagrams for the molecules used here. Relaxation rates are also indicated. W_e and W_n are electron and nitrogen relaxation rates, and K_x is the Heisenberg exchange rate. Experimental variation of the concentration permits separation of Heisenberg exchange from nuclear relaxation. If a short pulse is delivered to the 1–2 transition of the ^{15}N species and the time dependence of the m_z component of magnetization of this transition is observed indirectly by a weak incident microwave level, the signal is given by Eq. (1), and if the population difference of the 3–4 transition is observed (SR ELDOR), by Eq. (2) [24]:

$$i_{1,2} = I_1\left[e^{-2W_e t} + 2e^{-(2W_e+3W_n+NK_x)t}\right], \quad (1)$$

$$i_{3,4} = I_1\left[e^{-2W_e t} - e^{-(2W_e+3W_n+NK_x)t}\right]. \quad (2)$$

Here, *N* is the spin-label concentration. I_1 is a constant to be defined by initial conditions. If a long pulse is used, the relative intensities of the two exponentials change. However, time constants do not depend on pulse characteristics. Note the difference in signs of the double exponentials for SR EPR and SR ELDOR. The use of long pulses in SR decreases the amplitude of the second exponential, which is desirable if the goal is to measure W_e. For SR ELDOR, short pulses are generally used.

Eqs. (3)–(5) provide similar results for a short pulse that pumps interval 1–2 of the ^{14}N energy-level diagram [24]. It is interesting to note that the authors of Ref. [24] were experimentally able to assign triple exponentials under the assumption that the number of exponentials must agree with these equations:

$$i_{1,2} = I_1\left[e^{-2W_e t} + 3/2e^{-(2W_e+W_n+NK_x)t} + 1/2e^{-(2W_e+3W_n+NK_x)t}\right], \quad (3)$$

$$i_{3,4} = I_1\left[e^{-2W_e t} - e^{-(2W_e+3W_n+NK_x)t}\right], \quad (4)$$

$$i_{5,6} = I_1\left[e^{-2W_e t} - 3/2e^{-(2W_e+W_n+NK_x)t} + 1/2e^{-(2W_e+3W_n+NK_x)t}\right]. \quad (5)$$

For a short pulse on the central line, interval 3–4, double exponentials are obtained, Eqs. (6) and (7), for both SR EPR ($i_{3,4}$) and SR ELDOR ($i_{1,2}$ and $i_{5,6}$):

$$i_{3,4} = I_1\left[e^{-2W_e t} + 2e^{-(2W_e+3W_n+NK_x)t}\right], \quad (6)$$

$$i_{1,2} = i_{5,6} = I_1\left[e^{-2W_e t} - e^{-(2W_e+3W_n+NK_x)t}\right]. \quad (7)$$

Percival and Hyde [25] carried out a general analysis of the SR experiment by solving the Bloch equations for an arbitrary initial magnetization and a steady-state value of weak observing microwave field. Terms m_x and m_y, if they are present following the saturating pulse, give rise to intense free induction decay (FID). For narrow EPR lines, the FID signal can contaminate the SR signal and means are required for its suppression. This issue is discussed in detail in Ref. [25].

Percival and Hyde also found that the level of the observing power can affect the value of the time constant for SR, Eq. (8), where $b = \gamma_e B_1$:

$$m_y(t)/m_z \propto e^{-\left[(T_{1e})^{-1}+b^2T_{2e}\right]t}. \quad (8)$$

The true T_{1e} value is found by extrapolating the observed time constant to zero observing power. Of course, the SR signal intensity is higher if high observing power is used. Yin and Hyde [26] pointed out that *changes* in the observed T_{1e} arising from bimolecular collisions with dissolved oxygen are reliable monitors of oxygen transport even if the observing power is high.

1.4. Relaxation mechanisms

Robinson and co-workers [14,27] developed a comprehensive theory of electron and nuclear spin–lattice relaxation of spin labels in solution. They also provide extensive validation of the theory at *X*-band using SR EPR and SR ELDOR. The *X*-band studies were over a wide range of rotational correlation times, τ_c. Several possible relaxation mechanisms were considered, and experimental measurements permitted determination of dominant mechanisms. The microwave frequency in radians per second, ω_0, appears in the theory, and variation of frequency provides an additional opportunity to validate and extend the analysis. See Refs. [17,28,29].

2. Methods

2.1. Spectrometer system

The microwave bridge circuit is depicted in Fig. 3. The overall multi-arm bridge configuration is based on the double-sideband fixed-filter approach previously developed at *X*-band [30] and *Q*-band [17]. Multi-arm bridges enable multiple frequency experiments such as multiquantum (MQ) EPR and MQ ELDOR. We extend this technological approach to *W*-band SR EPR and SR ELDOR in this work. In the overall approach, mixers are used to generate double-sideband suppressed-carrier frequencies. Fixed-tuned filters are then used to select the desired sideband and suppress the residual carrier and the undesired sideband by greater than 50 dB. Hence, one spectrally pure frequency is generated in each arm. The frequencies from the incident power arms are combined and directed to the sample resonator.

The multi-arm bridges at *X*-band and at *Q*-band utilize a single frequency translation from each synthesizer output to the microwave frequency of the corresponding arm. Low phase noise synthesizers with a common time-base are utilized in the generation of the multiple time-locked frequencies. The *W*-band microwave bridge circuit in this work uses two frequency translations in each arm. The two-step frequency translation strategy permits convenient frequency adjustment of multiple time-locked distinct frequencies without compromising phase-noise performance.

The *W*-band bridge in Fig. 3 is similar to the configuration previously utilized in continuous wave (CW) frequency-modulation experiments [18] but contains an additional incident-frequency arm. The two frequency translations are from a synthesizer frequency, nominally 2 GHz to 35 GHz, and from 35 to 94 GHz. The *Q*-band microwave oscillator is nominally set at 33 GHz. The *Q*-band stage contains two incident-frequency arms and a reference arm, each with a separate synthesizer that is time-locked to the others. The synthesizers in the observe (OBS Arm) and pump (PUMP Arm) arms (see Fig. 3) are nominally set to 2 GHz for upconversion of the 33 GHz microwave oscillator output to 35 GHz. The utilization of a frequency translation approach provides significant ease and flexibility in setting the relative observe arm and pump arm frequencies. They are separately set by the synthesizers in each arm, typically a few kHz apart for SR to suppress the FID signal, and for SR ELDOR to the spacing of two lines, usually on the order of 30 MHz. Normally, the pump rather than the observe is offset from the 2 GHz synthesizer center frequency for proper receiver operation (described later). The observe arm power is turned off for detection of FID. The pump and observe frequencies are time-locked in this bridge configuration.

Utilization of a frequency translation approach is also advantageous for pulse formation. Instead of formation at the nominal microwave frequency of the experiment, the pulses are formed by switching the 2 GHz pump arm synthesizer feed to the pump arm upconversion mixer to *Q*-band (see Fig. 3). The *Q*-band pump pulse is then translated to *W*-band. Component quality for pulse formation is significantly higher at 2 GHz relative to *W*-band.

The *Q*-band frequencies are translated to *W*-band in upconversion "*Q*-band to *W*-band" (*Q* to *W*) mixers. The *V*-band local oscil-

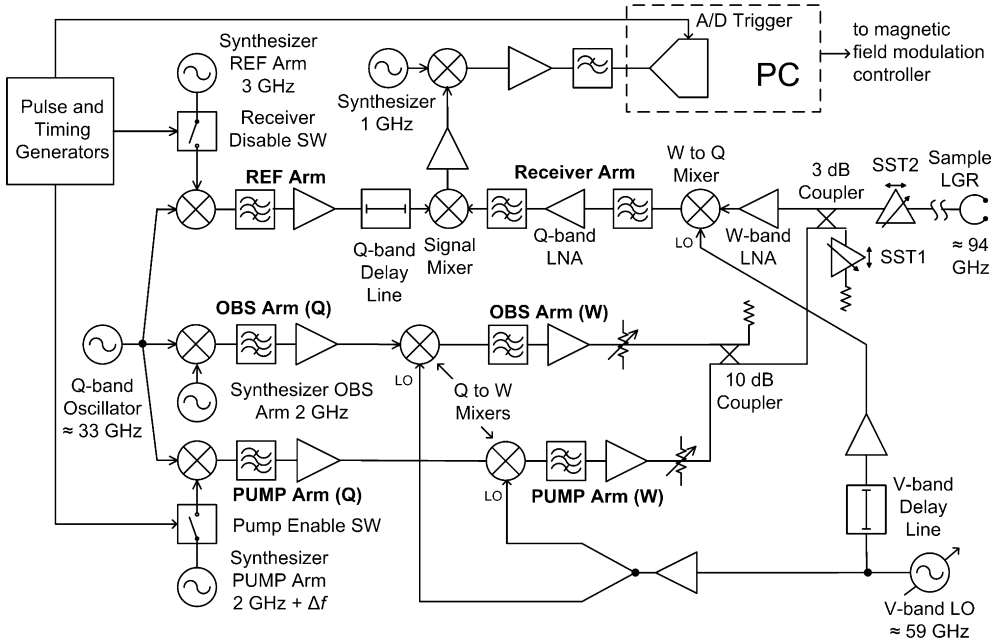

Fig. 3. Block diagram of the *W*-band SR EPR bridge configuration. Numerous isolators and interconnection components are not shown for clarity.

lator (LO) frequency supplied to these mixers is nominally set to 59 GHz. The *W*-band frequency is set by adjusting the frequency of the *V*-band local oscillator, not the IF frequency from the *Q*-band system. The mechanical tuner on the commercial *V*-band oscillator (Terabeam, North Andover, MA) is used for coarse frequency adjustments. The full 3 GHz tuning range of the *V*-band oscillator is translated to *W*-band. The oscillator also has an input port at which a voltage can be introduced to a varactor for fine frequency adjustments and for automatic frequency control (AFC) operation.

The *Q*-band portion of the microwave bridge is maintained at constant frequency. This approach keeps the *Q*-band frequency near the center of the 1 GHz bandwidth of the *Q*-band portions of the bridge, which is desirable for accommodating the bandwidths of pulsed microwave signals. Path length equalization and AFC operation are accomplished at *V*-band. The delay line is in the *V*-band LO waveguide circuit, not the *W*-band circuit. The resulting stability and ease of frequency tuning are significant attributes in a multi-arm millimeter-wave bridge configuration.

This is the first report of path length equalization in a *W*-band bridge to the best of our knowledge. Path length equalization is essential when low-*Q* resonators, such as LGRs, are used. Otherwise, frequency-dependent phase variations between the signal paths of an unbalanced bridge result in an interference pattern over the bandwidth of the resonator, and this makes bridge setup, stability, and operation problematic.

The *W*-band frequencies are individually amplified and then combined in a 10 dB directional coupler (see Fig. 3). The combined incident frequencies feed the *W*-band sample resonator via a 3-dB coupler (Fig. 3). This coupler assembly has two slide screw tuners (SST), labeled SST1 and SST2, that are used in the resonator setup procedure. The resonator is initially replaced with a termination, and the SST on the load port of the 3 dB Coupler (Fig. 3; SST1) is adjusted to suppress directional coupler leakage (including reflections from waveguide flanges) to maintain a flat reflection baseline across the resonator bandwidth. It is not necessary to adjust SST1 again over the course of the experiment. The in-line SST (Fig. 3; SST2) is adjusted as needed to achieve and maintain resonator match over the course of the experiment. Once the resonator setup procedure is complete, sample changes usually require a small adjustment of SST2. This adjustment can be made quickly because SST2 is easily accessed on the *W*-band assembly external to the magnet.

The 3 dB directional coupler is interfaced to the sample resonator by a low-loss coin-silver WR-10 waveguide of 0.90 m length. The resonator is a five-loop–four-gap LGR [16]. The LGR is positioned into a Magnex Split Pair EPR Superconducting Magnet System (Oxford, UK) via a side access port, which is advantageous for room temperature sample handling and to minimize waveguide path lengths. An Oxford Instrument room-temperature sweep coil power supply (Model IPS120-10) is used to set the nominal magnetic field at the sample resonance.

The EPR signal is amplified in a *W*-band low-noise amplifier (LNA), downconverted back to *Q*-band in a *W* to *Q* mixer, and amplified by a *Q*-band LNA. The LO frequency that feeds the *W* to *Q* downconversion mixer is the same *V*-band LO frequency that feeds the *Q* to *W* upconversion mixers. Hence, the received signal is returned to the nominal frequency of 35 GHz. The *Q*-band signal is downconverted to 1 GHz by mixing with 36 GHz from the *Q*-band reference arm, noting that the synthesizer that drives the reference arm is set to 3 GHz. This multiple downconversion approach overcomes the high $1/f$ noise that would be present in the *Q*-band signal mixer in a single downconversion approach. This approach permits use of a fixed-frequency I/Q mixer at 1 GHz. The 1 GHz signal is downconverted to baseband by mixing with the output of a 1-GHz synthesizer. The baseband EPR signal is amplified, filtered by a selectable low pass filter, and digitized by an Acqiris (Agilent) PCI Signal Analyzer Model AP240-Augr analog-to-digital (A/D) card in a personal computer (PC), which completes the signal processing. The A/D card can be set for further filtering of the incoming signal.

The entire microwave circuit rests on an air-bearing supported table that slides on a granite slab for convenient access of the resonator to and from the magnet.

The pulse and timing generators consist of a time-locked Stanford DS-345 synthesizer that triggers two Stanford DG-535 delay/pulse generators (Stanford Research Systems, Sunnyvale, CA). They drive the 2 GHz pump enable PIN diode switch (SW), the 3 GHz receiver disable PIN diode switch, and the A/D trigger. The receiver must be disabled during the pump pulse; otherwise, the residual signal from the reflection of the pump from the resonator overloads the baseband signal processing chain, which cannot recover before the data collection commences. See the timing diagram, Fig. 4, and the circuitry in the upper left of Fig. 3.

Signal processing proceeds as follows: the individual decays resulting for each pump pulse while on resonance are digitized and added together. The resultant signal averaging improves the signal-to-noise ratio. The magnetic field is shifted on and off resonance by applying a square wave to the field modulation coils. An identical number of decays is collected in the off resonance condition. This forms a baseline that is then subtracted from the on resonance sum to cancel instrumental artifacts. The resulting decays are analyzed in a curve fitting program to give amplitude and time-constant information.

2.2. Loop-gap resonator

We have introduced an improvement over the *W*-band LGR assembly described in Ref. [16]. Small water-cooled plates were attached to the assembly, and since the silver LGR is in good thermal contact, all parts of the assembly are clamped to the temperature of the water bath. Conductive, convective, and radiation sources contribute to the thermal environment. By clamping the assembly to a thermal bath, substantially improved system stability was achieved.

The combination of the LGR [16] and high nominal frequency (*W*-band) present significant advantages for SR EPR and SR ELDOR. As with CW EPR, the low *Q*-factor inherently suppresses source phase noise and is less sensitive to frequency drift between the incident frequency and the resonator frequency. Operation without AFC has been shown to be feasible for data collection times on the order of several minutes. Unlike SR ELDOR at lower frequencies, the low *Q* allows both the pump and observe frequencies to be well within the resonator bandwidth.

This LGR with a water sample has a loaded *Q* factor of approximately 100. The resonator efficiency parameter of the *W*-band LGR, Λ, with aqueous sample of 0.15 mm i.d. was calculated to be 8.2 using High Frequency Structure Simulator (HFSS) (Ansoft,

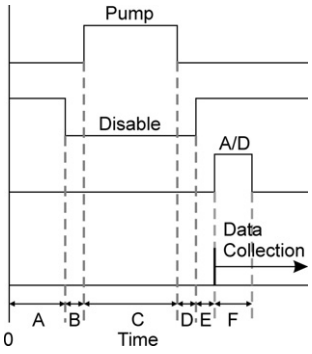

Fig. 4. Timing diagram.

Pittsburg, PA). For 0.20 mm i.d., Λ drops sharply to 4.9. The smaller diameter sample tube is highly advantageous for SR experiments. The maximum incident pulse power on the LGR in the apparatus described here is 5 mW, corresponding to about 1 G in the rotating frame. High Λ and high bandwidth were found to be mutually beneficial in the SR EPR experiments described here: neither a PIN diode protection component prior to the *W*-band LNA nor use of a bimodal resonator is required. One consequence of high Λ and low resonator *Q* is that the dead-time between the end of the pulse and the start of data collection is reduced because there is less stored energy in the resonator when the pulse ends.

The process of changing samples, insertion of the LGR into the magnet bore, and subsequent adjustment of SST2 is fast and easily accomplished. As previously noted, temperature changes of the sample/LGR are achieved by changing the temperature of the bath water pumped through the LGR assembly cooling plates. A 10-degree change in the set temperature of the water bath requires 20 min for stabilization of the sample/LGR temperature and the coupling and resonant frequency of the LGR.

In summary, the unique features of this spectrometer are the multi-arm multi-frequency capability, path length equalization, two-stage frequency translation, low-*Q* LGR, pulse formation at 2 GHz, and convenient sample exchange.

2.3. Sample preparation

All samples for data reported here were under nitrogen. Two methods of removing oxygen were used: one by gas exchange using a PTFE sample tube and one in a quartz capillary in which degassed sample was transferred under nitrogen. Results were indistinguishable. Two concentrations were used, 0.1 and 0.5 mM, for the CTPO and TEMPONE samples.

A control experiment was carried out to verify that traces of oxygen remaining in the quartz capillaries were insufficient to affect the measured relaxation times significantly. The ^{15}N version of CTPO, compound I with methyl groups deuterated, was used in a PTFE sample tube. Values of T_{1e}^{-1} as a function of oxygen concentration in an exchange gas flowing over the sample were extrapolated to zero oxygen concentration by a linear fit to the data. The measured relaxation rate at zero oxygen concentration using the extrapolation method was about 15% *greater* than values measured for the 0.5 and 0.1 mM samples in quartz capillaries, and the rate actually measured at zero oxygenation concentration in PTFE was within 1% of the values in quartz capillaries. The experiment supports the adequacy of the deoxygenation methods, although it does suggest small errors in the calibration of the gas blender that was used to mix the exchange gas.

3. Results

3.1. Free induction decay

The EPR spectrum from ^{15}N-deuterated methyls-CTPO is shown in Fig. 5, and the FID signals in Fig. 6a and b. In these experiments,

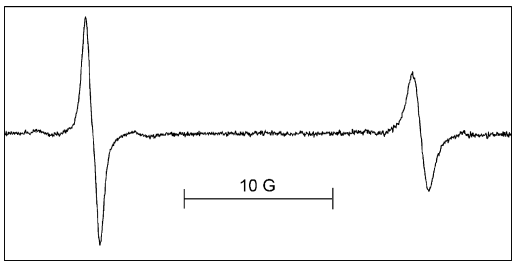

Fig. 5. *W*-band EPR spectrum of ^{15}N CTPO.

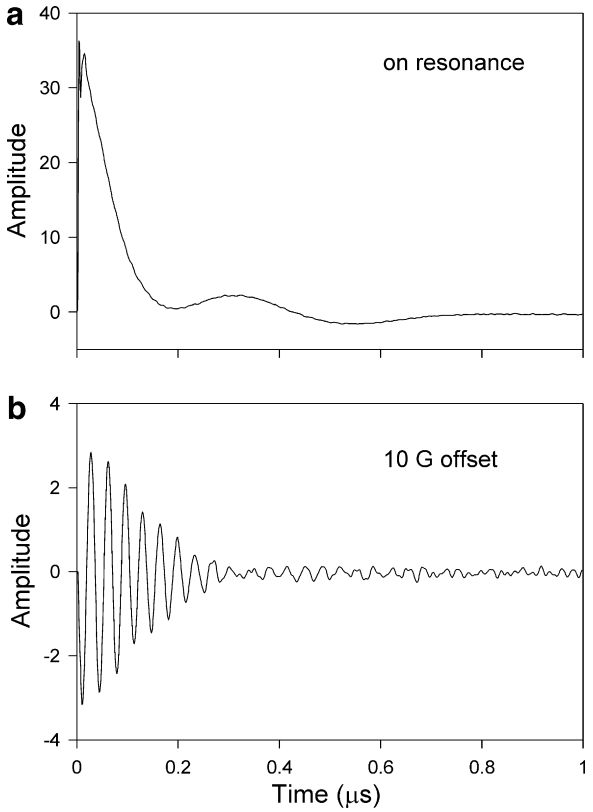

Fig. 6. Free induction decays from 0.1 mM ^{15}N CTPO under nitrogen at 93.80 GHz, data sets are 2048 points, pulse width 0.3 μs, power level ~3 mW: (a) approximately on resonance 2.1×10^6 averages on and off resonance; (b) 10 G offset 3.5×10^6 averages on and off resonance.

the frequencies of the microwave pulse and the microwave reference are the same, and there is no observe power. In Fig. 6a, the polarizing magnetic field was set to the low field transition. Analysis of the spectrum shows that the field position was, in fact, slightly off-center. A Fourier Transform reveals a spectral line that is partially split by coupling to the ring proton but otherwise contains no features. This is a direction for future research. The data for Fig. 6a were obtained in 42 s and for Fig. 6b in 70 s. The high sigmal-to-noise ratios are felt to be notable. The Fourier Transform yields pure EPR absorption and pure dispersion lineshapes, which is advantageous in comparison with the derivative-like lineshapes obtained when magnetic field modulation is used. It is noted that Hofbauer et al. [8] also report FIDs from a small nitroxide in water at 94 GHz.

Fig. 6b is an FID signal obtained when the magnetic field is 10 G (28 MHz) off resonance. It is weaker in intensity by a factor of 10 compared with Fig. 6a. Presumably, the tip angle for Fig. 6a was small. The incident microwave power for the experiments of Fig. 6 was the same as used for SR EPR and SR ELDOR, and the pulse durations were similar. There was no effort to optimize the FID signals. Fig. 6 establishes that it is important to suppress FID signals when carrying out SR experiments. It also establishes that FID detection is feasible as a means to carry out EPR experiments, particularly at *W*-band using an LGR.

3.2. SR EPR and SR ELDOR of CTPO and TEMPONE

Dependances of apparent T_{1e} on observed power were difficult to detect. This may be because of the appearance of T_2 in Eq. (8). Line broadening is apparent in Fig. 5. This point was made previously in an SR experiment at *Q*-band [17]. Observing microwave

powers can be higher in spin labels in viscous solution or at high microwave frequencies because of shorter T_2 values, which improves the signal-to-noise ratio.

Fig. 7a and b shows a representative SR EPR signal and a representative SR ELDOR signal of CTPO, respectively. Experimental conditions are in the figure caption. The novel method of FID suppression introduced in Ref. [17] was used for SR EPR—namely separating the pump and observe microwave frequencies by a frequency of the order of 1 kHz. SR EPR and SR ELDOR signals were fit to double exponentials according to Eqs. (1), (2), (4), (6), or (7), where the first has a time constant T_{1e} and the second is designated T_b.

Table 1 gives values for the electron spin–lattice relaxation time using SR EPR and SR ELDOR for both ^{14}N and ^{15}N forms of CTPO. For ^{15}N CTPO, there are four independent measurements in Table 1 for electron spin–lattice relaxation time. The average value is 1.48 μs. In addition, there are two independent measurements of T_b for 0.5 mM concentration, 0.55 and 0.53 μs, yielding an average value of 0.54 μs. Similarly, the average value of T_b for 0.1 mM concentration is 0.865 μs.

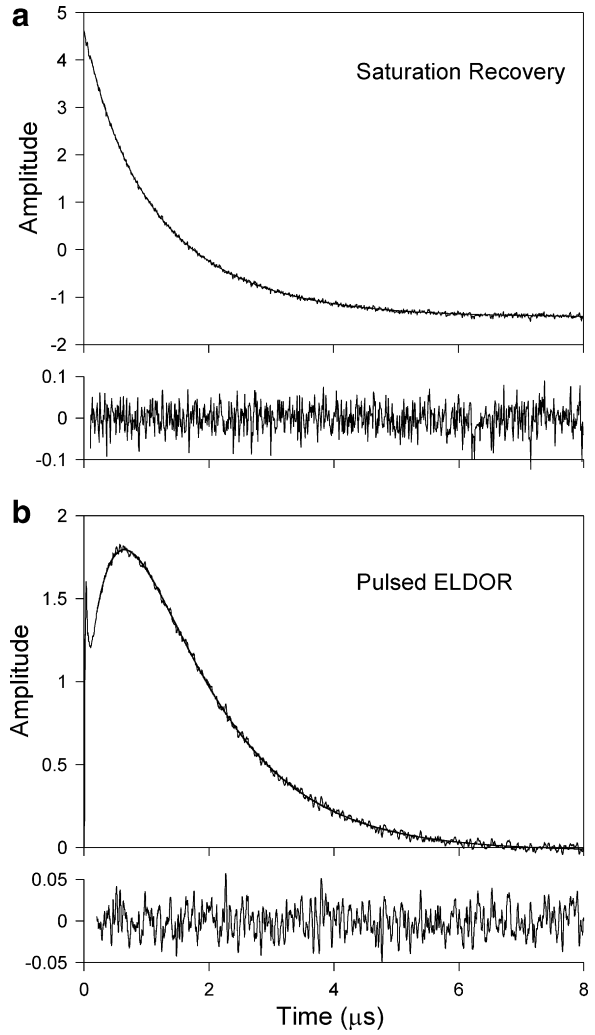

Fig. 7. Representative (a) SR EPR and (b) SR ELDOR signals for 0.5 mM ^{15}N CTPO. For SR 1024 points per record, 6.5×10^5 averages on resonance minus 6.5×10^5 averages off resonance, total acquisition time 26 s, pulse width 1 μs, pump power 3 mW, observe power 0.015 mW, high field line observed 94.02 GHz. For SR ELDOR parameters were the same except 8192 per record, 2.2×10^6 averages both on and off resonance, total acquisition time 91 s, pump width 0.3 μs on low field line. Separation of pump and observe 62.17 MHz. Best fit is overlaid and residuals are shown. See Tables 1 and 2 for relaxation times and rates.

Table 1
Relaxation times (μs) at *W*-band for small nitroxides

	SR EPR		SR ELDOR	
	T_{1e} (μs)	T_b (μs)	T_{1e} (μs)	T_b (μs)
^{15}N CTPO 0.5 mM	1.55	0.55	1.46	0.53
^{15}N CTPO 0.1 mM	1.50	0.88	1.40	0.85
^{14}N CTPO 0.5 mM	1.24	0.42	1.24	0.44
^{14}N CTPO 0.1 mM	1.28	0.67	1.24	0.71
^{14}N TEMPONE 0.5 mM	0.83	—	0.85	0.75
^{14}N TEMPONE 0.1 mM	0.83	—	0.88	0.79

Shorter T_{1e} values for the ^{14}N isotope of CTPO are thought to arise from the greater nitrogen nuclear quantum number and not from the nitrogen nuclear quadrupole coupling. For the ^{15}N form, the low field line was observed (Fig. 5) because of its greater intensity. The general theory from rate equation analysis indicates that for the ^{14}N form a triple exponential recovery is expected when observing the low field line (see Eq. (3)). We wished to avoid this situation and therefore observed the central line (Eq. (4)).

From either Eq. (1) or Eq. (2), one can write:

$$T_b^{-1} = T_{1e}^{-1} + T_{1n}^{-1} + T_x^{-1}, \tag{9a}$$

where T_x is the time constant for Heisenberg exchange. Equivalently,

$$T_b^{-1} = 2W_e + 2W_n + K_x, \tag{9b}$$

where K_x is the Heisenberg exchange rate as defined in Fig. 2. The spin-label concentration N appearing in Eqs. (1)–(7) has been set to 1 for convenience in Fig. 2. Since we have data at two concentrations, two independent equations in two unknowns can be written:

$$(0.54)^{-1} = (1.48)^{-1} + 2W_n + 5K_x, \tag{10}$$

$$(0.865)^{-1} = (1.48)^{-1} + 2W_n + K_x. \tag{11}$$

Solutions are $K_x = 0.17 \times 10^6$ collisions per second at a concentration of 10^{-4} M (i.e., $T_x = 5.88$ μs) and $W_n = 0.155 \times 10^6$ nitrogen nuclear relaxation events per second (i.e., $T_{1n} = 3.23$ μs), noting that each such event changes the population difference of the relaxing states by 2.

Similarly, for ^{14}N CTPO using Eqs. (4)–(6), or (7), one can write:

$$T_b^{-1} = T_{1e}^{-1} + 3W_n + K_x. \tag{12}$$

Equations analogous to Eqs. (10) and (11) are:

$$(0.43)^{-1} = (1.25)^{-1} + 3W_n + 5K_x, \tag{13}$$

$$(0.69)^{-1} = (1.25)^{-1} + 3W_n + K_x. \tag{14}$$

We obtain $K_x = 0.22 \times 10^6$ collisions per second, in fair agreement with the value of 0.17×10^6 found for the ^{15}N isotope, and $W_n = 0.14$ (i.e., $T_{1n} = 2.33$ μs). Relaxation rates and times are summarized in Table 2.

For TEMPONE we were unable to obtain a reliable fit for a double exponential from the SR EPR data. This apparently was because a very long saturating microwave pulse, 5 μs, was used, which suppressed the intensity of the second exponential. An average of the four independent measurements of T_{1e} for TEMPONE from SR EPR

Table 2
Relaxation times (μs) and rates ($\times 10^{-6}$)[a]

	T_{1e}	W_e	T_{1n}	W_n	T_x	K_x
^{15}N CTPO	1.48	0.34	3.23	0.155	5.88	0.17
^{14}N CTPO	1.25	0.40	2.33	0.14	4.54	0.22
^{14}N TEMPONE	0.85	0.59	—	—	—	—

[a] Standard deviations for T_{1e} and W_e are estimated to be ±3%.

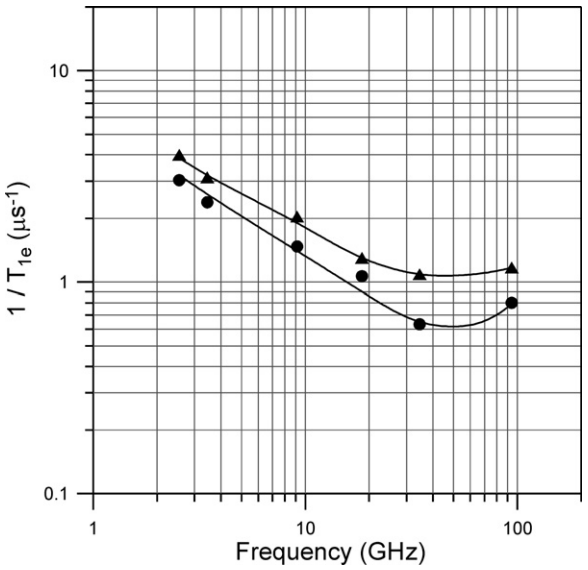

Fig. 8. Microwave frequency dependence of the electron spin–lattice relaxation rate T_{1e}^{-1} of ^{14}N CTPO (circles) and TEMPONE (triangles) in water. The *W*-band relaxation rates and standard deviations are T_{1e}^{-1} (CTPO) = 0.80 ± 0.03 (μs)$^{-1}$ and T_{1e}^{-1}(TEMPONE) = 1.18 ± 0.03 (μs)$^{-1}$.

and SR ELDOR, each at two concentrations, yields 0.85 μs. For the SR ELDOR experiment on TEMPONE, a saturating pulse of 0.3 μs was used. The values of T_b that were obtained for both concentrations are the same within the range of experimental errors exhibited by the data of Table 1, and these values are within 0.1 μs of the measured values for T_{1e}. Apparently, both Heisenberg exchange rates and nitrogen nuclear relaxation rates are slow relative to the electron spin–lattice relaxation rate. Because of experimental error, the data do not support algebraic separation of W_n and K_x for TEMPONE.

The value obtained for T_{1e} for the ^{14}N form of CTPO has been combined with previously obtained multifrequency measurements [17] in Fig. 8. A remarkable fact is that the value obtained at 94 GHz departs strongly from the trend observed using data obtained at lower frequencies. The relaxation rate increases with frequency comparing 35 with 94 GHz results, which is inconsistent with relaxation mechanisms previously considered for the microwave frequency dependence of the spin–lattice relaxation time of free radicals in solution [14,27]. SR experiments on TEMPONE, compound III of Fig. 1, are also plotted in Fig. 8. As noted previously, it has a six-member ring in contrast to CTPO with a five-member ring and one double bond. Results for CTPO and TEMPONE are similar throughout the microwave frequency range of 2.5–94 GHz. The spin–lattice relaxation rates of TEMPONE and CTPO in the range of 2.54–34.6 GHz exhibit a dependence on frequency that varies approximately as $\omega_0^{-1/2}$ (see Fig. 8).

4. Discussion

Alternative methods of microwave bridge design were considered. One of these was a homodyne bridge where a *W*-band fundamental oscillator would be employed. However, it is difficult to generate multiple time-locked frequencies with fundamental sources at 94 GHz. If a single frequency translation from the synthesizer frequency to the *W*-band frequency were to be utilized, which is the heterodyne approach, the nominal frequency of the synthesizers would be a minimum of 4 GHz due to *W*-band filter-design constraints. The higher frequency synthesizers and the associated 90 GHz microwave oscillator would both contribute to elevated phase noise levels. Frequency multiplication is another possibility. However, the phase noise is severely compromised by a degradation factor of $20\log(94/f_{in})$ [31]. We concluded that the two-stage frequency translation approach is preferable.

Interest in SR measurements on nitroxide radical spin labels lies primarily in determination of bimolecular collision rates with dissolved oxygen and paramagnetic metal ions. Oxygen and metal ion accessibility measurements are a primary experimental tool for molecular structure studies in a context of site-directed spin-labeling [5]. In addition, the discrimination by oxygen transport (DOT) method [32] has proven useful in probing membrane structure. It is based on the observation that oxygen solubilities in membrane domains can differ even though spin-label motion does not. In these studies, the CW saturation method is most often used, even though the results depend not only on T_{1e} but also on T_2. CW measurements fingerprint the bimolecular collision rate between paramagnetic species and spin labels, while SR methods provide a quantitative measurement. CW methods become increasingly problematic as spin-label motion slows or the microwave frequency increases, resulting in spectra that are in the so-called slow tumbling domain with very short T_2 values.

In this prototypical SR investigation at *W*-band, CTPO, a small hydrophilic spin probe, was studied extensively. At *X*-band in water, it is in the motionally narrowed regime where resolved superhyperfine structure can be used for oximetric purposes. This resolution is lost at *W*-band. The oximetric method of Halpern et al. [23] no longer works at *W*-band (see Fig. 5). This method depends on methyl group deuteration and motional narrowing that permits resolution of the doublet arising from the ring proton of CTPO (see compound I, Fig. 1). At *X*-band, bimolecular collisions with oxygen decrease the resolution, which can be used as a metric for oxygen concentration. Resolution of the proton coupling is not seen at *W*-band. For measurements of concentration of oxygen in water at *W*-band, the methods of this paper provide quantitative data.

In the studies reported here, variation of sample concentration led to the conclusion that both Heisenberg exchange and nitrogen nuclear relaxation must be considered when using small hydrophilic spin probes at a concentration of 0.1 mM and higher.

There are three ELDOR mechanisms of interest: (i) nitrogen nuclear relaxation, T_{1n}, and (ii) Heisenberg exchange, which have been studied here, and (iii) slow rotational diffusion that carries saturation from one portion of the spectrum to another on the time scale of T_{1e} [33]. Time resolved ELDOR permits separation of these mechanisms. The study of anisotropic motions at high microwave frequencies (mechanism [iii]) is a particularly promising application of the methods since the nitrogen nuclear relaxation time becomes very long as motion slows and the spectral shape becomes indistinguishable from the rigid limit spectrum.

The sign change in the two exponential decays comparing SR EPR with SR ELDOR (see the Theory section) permits measurement of both terms over a wide range of relative decay rates. In this study, we have not investigated in detail those situations where three exponentials are expected (Eqs. (3) and (5)). SR ELDOR is a preferred technique in this circumstance.

For samples studied here, no error in sample preparation can occur for measurement of T_{1e} other than failure to exclude oxygen. Error in radical concentration affects the Heisenberg exchange rate, but not other relaxation rates. The primary measurement error is the use of too much microwave power. The computer fit of the model to the data depends on the signal-to-noise ratio. The quality of the SR fits is also degraded when double exponential relaxation occurs with similar but not identical relaxation rates. ELDOR can be useful, as can variation of radical concentration, in the circumstance that T_{1e} and T_b are similar.

Measurement of T_{1n} can be an experimental challenge because this time becomes very short when $\omega_0\tau_c \sim 1$, Eq. (10). SR ELDOR

would seem to be an ideal technique, but improved pulse technology is required.

For CTPO, the FID signal is readily obtained at *W*-band with excellent signal-to-noise ratio. As the motion slows, T_2 values and FIDs become short, and precise delivery of short $\pi/2$ pulses will be required.

The *W*-band LGR [16] is the enabling technology for the experiments described here. The active region of the resonator is about 1 wavelength. The field along this length is reasonably uniform and can be improved further by introducing Uniform Field LGR technology [34]. The instrument as it is presently configured works well for T_{1e} measurements in both the SR EPR and SR ELDOR modes of operation.

The break in the trend of relaxation rate versus microwave frequency (Fig. 8) requires further investigation. Studies were carried out with consistent results on two spin labels at two concentrations and two isotopes using both SR and SR ELDOR by two different operators over a time period of about one month. Two methods of oxygen removal were employed with consistent results. All measurements were carried out as a function of incident observing microwave power. It is doubtful to the authors that some unknown experimental error has occurred. Hofbauer et al. [8] report unexpectedly short T_{1e} values for 1 mM solution of TEMPO in a 10% glycerol–water mixture at *W*-band and suggest a specific frequency-dependent relaxation mechanism involving dynamic modulation of the *g*-value. These authors call for more detailed studies, as do we.

Acknowledgments

This work was supported by Grants EB001417 and EB001980 from the National Institutes of Health. We thank Professor Howard J. Halpern for the gift of deuterated ^{15}N CTPO.

References

[1] S.S. Eaton, G.R. Eaton, Saturation recovery EPR, in: S.S. Eaton, G.R. Eaton (Eds.), Biomedical EPR—Part B: Methodology, Instrumentation, and Dynamics, Kluwer Academic/Plenum Publishers, New York, 2005, pp. 3–18.
[2] L.D. Kispert, Electron–electron double resonance, in: S.S. Eaton, G.R. Eaton (Eds.), Biomedical EPR—Part B: Methodology, Instrumentation, and Dynamics, Kluwer Academic/Plenum Publishers, New York, 2005, pp. 165–197.
[3] J.S. Hyde, ELDOR spectroscopy, in: G.R. Eaton, S.S. Eaton, K.M. Salikhov (Eds.), Foundations of Modern EPR, World Scientific, Singapore, 1998, pp. 577–586.
[4] J.S. Hyde, Saturation recovery, in: G.R. Eaton, S.S. Eaton, K.M. Salikhov (Eds.), Foundations of Modern EPR, World Scientific, Singapore, 1998, pp. 607–618.
[5] C.S. Klug, J.B. Feix, SDSL: a survey of biological applications, in: S.S. Eaton, G.R. Eaton (Eds.), Biomedical EPR—Part B: Methodology, Instrumentation, and Dynamics, Kluwer Academic/Plenum Publishers, New York, 2005, pp. 269–308.
[6] W.K. Subczynski, H.M. Swartz, EPR oximetry in biological and model samples, in: S.S. Eaton, G.R. Eaton, L.J. Berliner (Eds.), Biomedical EPR—Part A: Free Radicals, Metals, Medicine, and Physiology, Kluwer Academic/Plenum Publishers, New York, 2005, pp. 229–282.
[7] O.Y. Grinberg, L.J. Berliner (Eds.), Very High Frequency (VHF) ESR/EPR (Biological Magnetic Resonance 22), Kluwer Academic/Plenum Publishers, New York, 2004.
[8] W. Hofbauer, K.A. Earle, C.R. Dunnam, J.K. Moscicki, J.H. Freed, High-power 95 GHz pulsed electron paramagnetic resonance spectrometer, Rev. Sci. Instrum. 75 (2004) 1194–1208.
[9] W. Wang, R.L. Belford, R.B. Clarkson, P.H. Davis, J. Forrer, M.J. Nilges, M.D. Timken, T. Walczak, M.C. Thurnauer, J.R. Norris, A.L. Morris, Y. Zhang, Very high frequency EPR—94 GHz instrument and applications to primary reaction centers from photosynthetic red bacteria and to other disordered systems, Appl. Magn. Reson. 6 (1994) 195–215.
[10] M.J. Nilges, A.I. Smirnov, R.B. Clarkson, R.L. Belford, Electron paramagnetic resonance *W*-band spectrometer with a low-noise amplifier, Appl. Magn. Reson. 16 (1999) 167–183.
[11] P. Hofer, A. Kamlowski, G.G. Maresch, D. Schmalbein, R.T. Weber, The Bruker ELEXSYS E600/680 94 GHz spectrometer series, in: Very High Frequency (VHF) ESR/EPR (see Ref. [7]), pp. 401–429.
[12] K.A. Earle, A.I. Smirnov, High-field ESR: applications to protein structure and dynamics, HF ESR protein structure and dynamics, in: Very High Frequency (VHF) ESR/EPR (see Ref. [7]), pp. 96–135.
[13] J.S. Hyde, W. Froncisz, C. Mottley, Pulsed ELDOR measurement of nitrogen T1 in spin labels, Chem. Phys. Lett. 110 (1984) 621–625.
[14] B.H. Robinson, D.A. Haas, C. Mailer, Molecular dynamics in liquids: spin–lattice relaxation of nitroxide spin labels, Science 263 (1994) 490–493.
[15] D.A. Haas, T. Sugano, C. Mailer, B.H. Robinson, Motion in nitroxide spin labels: direct measurement of rotational correlation times by pulse electron double resonance, J. Phys. Chem. 97 (1993) 2914–2921.
[16] J.W. Sidabras, R.R. Mett, W. Froncisz, T.G. Camenisch, J.R. Anderson, J.S. Hyde, Multipurpose EPR loop-gap resonator and cylindrical TE_{011} cavity for aqueous samples at 94 GHz, Rev. Sci. Instrum. 78 (2007) 034701.
[17] J.S. Hyde, J.-J. Yin, W.K. Subczynski, T.G. Camenisch, J.J. Ratke, W. Froncisz, Spin label EPR T1 values using saturation recovery from 2 to 35 GHz, J. Phys. Chem. B 108 (2004) 9524–9529.
[18] J.S. Hyde, W. Froncisz, J.W. Sidabras, T.G. Camenisch, J.R. Anderson, R.A. Strangeway, Microwave frequency modulation in CW EPR at *W*-band using a loop-gap resonator, J. Magn. Reson. 185 (2007) 259–263.
[19] J.M. Backer, V.G. Budker, S.I. Eremenko, Y.N. Molin, Detection of the kinetics of biochemical reactions with oxygen using exchange broadening in the ESR spectra of nitroxide radicals, Biochim. Biophys. Acta 460 (1977) 152–156.
[20] T.J. Sarna, A.J. Duleba, W. Korytowski, H.M. Swartz, Interaction of melanin with oxygen, Arch. Biochem. Biophys. 200 (1980) 140–148.
[21] C.-S. Lai, L.E. Hopwood, J.S. Hyde, S. Lukiewicz, ESR studies of O_2 uptake by Chinese hamster ovary cells during the cell cycle, Proc. Natl. Acad. Sci. USA 79 (1982) 1166–1170.
[22] J.S. Hyde, W.K. Subczynski, Stimulation of ESR spectra of the oxygen-sensitive spin-label probe CTPO, J. Magn. Reson. 56 (1984) 125–130.
[23] H.J. Halpern, M. Peric, T.-D. Nguyen, D.P. Spencer, B.A. Teicher, Y.J. Lin, M.K. Bowman, Selective isotopic labeling of a nitroxide spin label to enhance sensitivity for T_2 oxymetry, J. Magn. Reson. 90 (1990) 40–51.
[24] J.-J. Yin, M. Pasenkiewicz-Gierula, J.S. Hyde, Lateral diffusion of lipids in membranes by pulse saturation recovery electron spin resonance, Proc. Natl. Acad. Sci. USA 84 (1987) 964–968.
[25] P.W. Percival, J.S. Hyde, Pulsed EPR spectrometer, II, Rev. Sci. Instrum. 46 (1975) 1522–1529.
[26] J.-J. Yin, J.S. Hyde, Use of high observing power in electron spin resonance saturation-recovery experiments in spin-labeled membranes, J. Chem. Phys. 91 (1989) 6029–6035.
[27] B.H. Robinson, A.W. Reese, E. Gibbons, C. Mailer, A unified description of the spin–spin and spin–lattice relaxation rates applied to nitroxide spin labels in viscous liquids, J. Phys. Chem. B 103 (1999) 5881–5894.
[28] R. Owenius, G.E. Terry, M.J. Williams, S.S. Eaton, G.R. Eaton, Frequency dependence of electron spin relaxation of nitroxyl radicals in fluid solution, J. Phys. Chem. B 108 (2004) 9475–9481.
[29] C. Mailer, R.D. Nielsen, B.H. Robinson, Explanation of spin–lattice relaxation rates of spin labels obtained with multifrequency saturation recovery EPR, J. Phys. Chem. A 109 (2005) 4049–4061.
[30] R.A. Strangeway, H.S. Mchaourab, J. Luglio, W. Froncisz, J.S. Hyde, A general purpose multiquantum electron paramagnetic resonance spectrometer, Rev. Sci. Instrum. 66 (1995) 4516–4528.
[31] W.P. Robins, Phase Noise in Signal Sources (IEE Telecommunications Series 9), Peter Peregrinus Ltd./Institution of Electrical Engineers, London, UK, 1982.
[32] I. Ashikawa, J.-J. Yin, W.K. Subczynski, T. Kouyama, J.S. Hyde, A. Kusumi, Molecular organization and dynamics in bacteriorhodopsin-rich reconstituted membranes: discrimination of lipid environments by the oxygen transport parameter using a pulse ESR spin-labeling technique, Biochemistry 33 (1994) 4947–4952.
[33] P. Fajer, D.D. Thomas, J.B. Feix, J.S. Hyde, Measurement of rotational molecular motion by time-resolved saturation transfer electron paramagnetic resonance, Biophys. J. 50 (1986) 1195–1202.
[34] R.R. Mett, J.W. Sidabras, J.S. Hyde, Uniform radio frequency fields in loop-gap resonators for EPR spectroscopy, Appl. Magn. Reson. 31 (2007) 571–587.